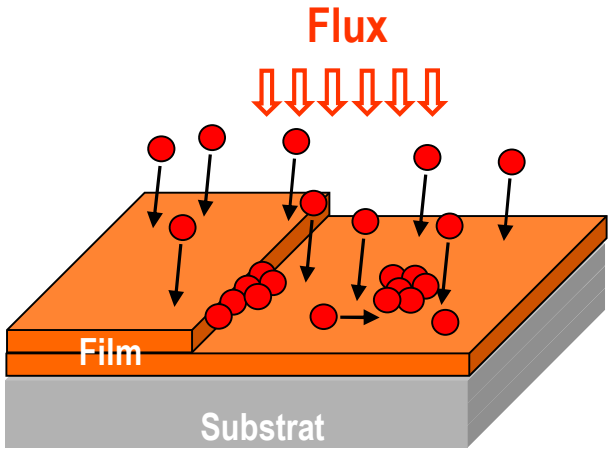
COnCOrD GdR 2081
COuplage méCanique Oxydation Diffusion

Journées Annuelles, 7-8 Juillet 2021

Genèse et relaxation des contraintes lors de la croissance de films minces polycristallins

Grégory Abadias

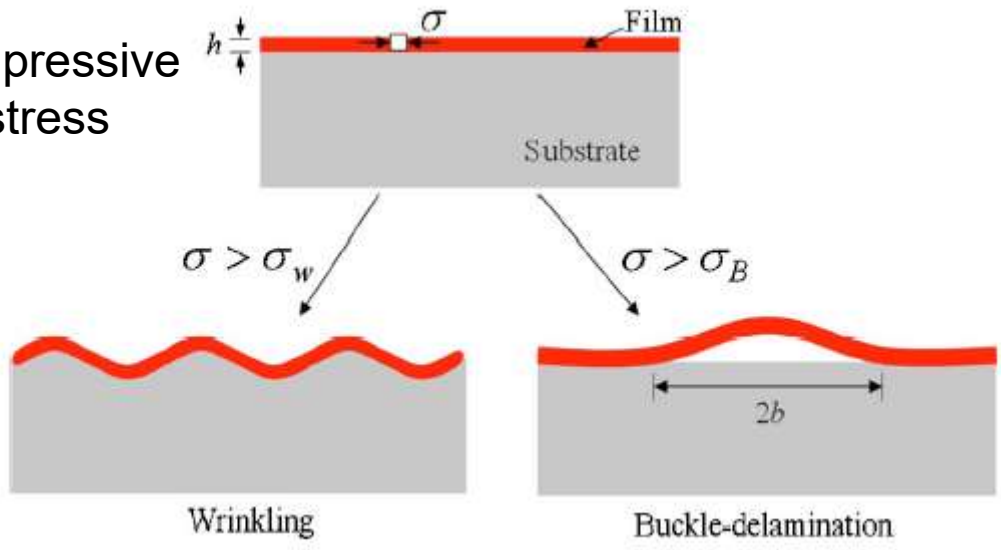
Institut P', CNRS-Université de Poitiers-ENSMA, France
Département Physique et Mécanique des Matériaux
gregory.abadias@univ-poitiers.fr

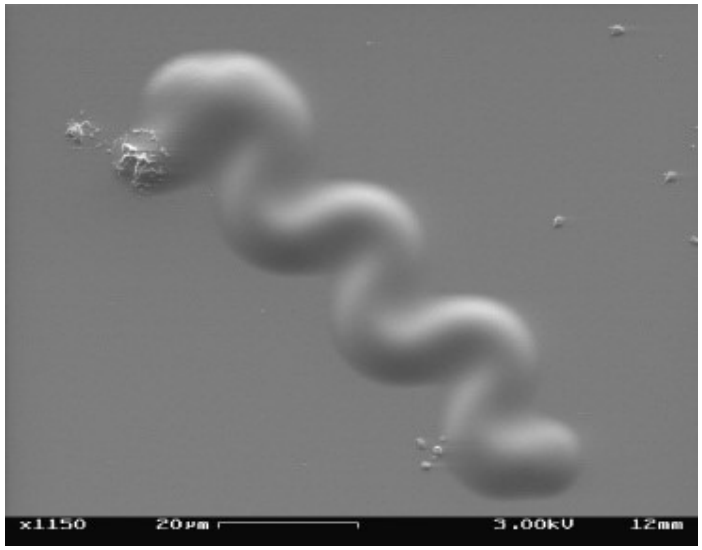


- Institut P' • UPR CNRS 3346
- SP2MI • Téléport 2
- Boulevard Marie et Pierre Curie • BP 30179
- F86962 Futuroscope-Chasseneuil- FRANCE

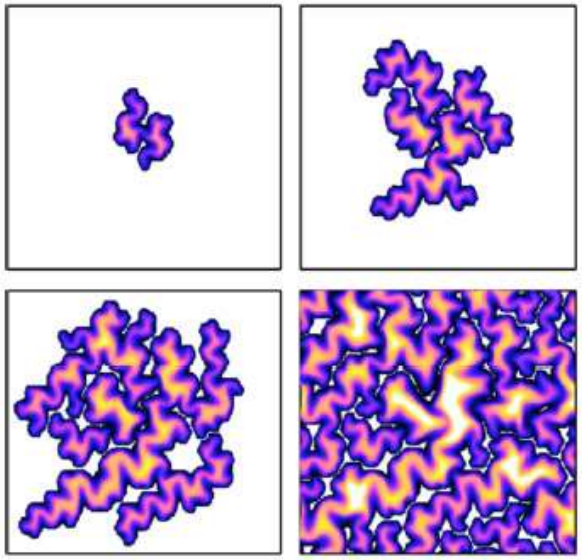
Introduction

compressive stress

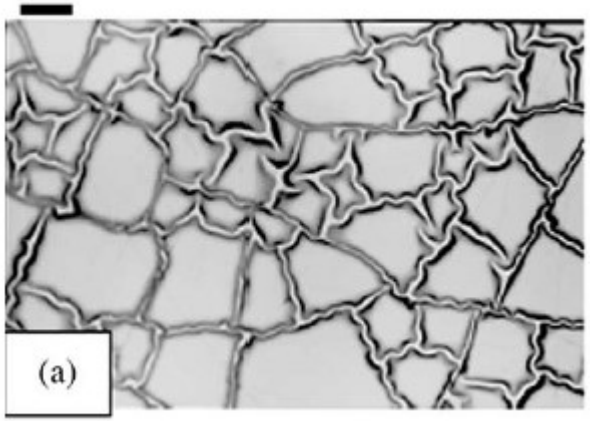


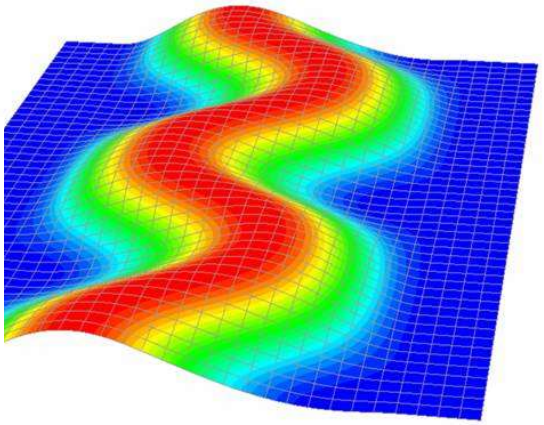


H. Mei et al., APL **90**, 151902 (2007)



E.A. Jagla, PBR **75**, 085405 (2007)

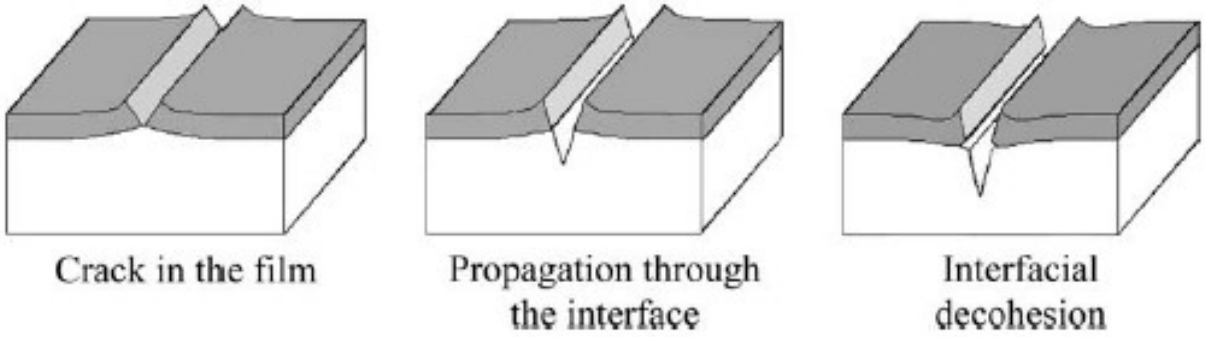


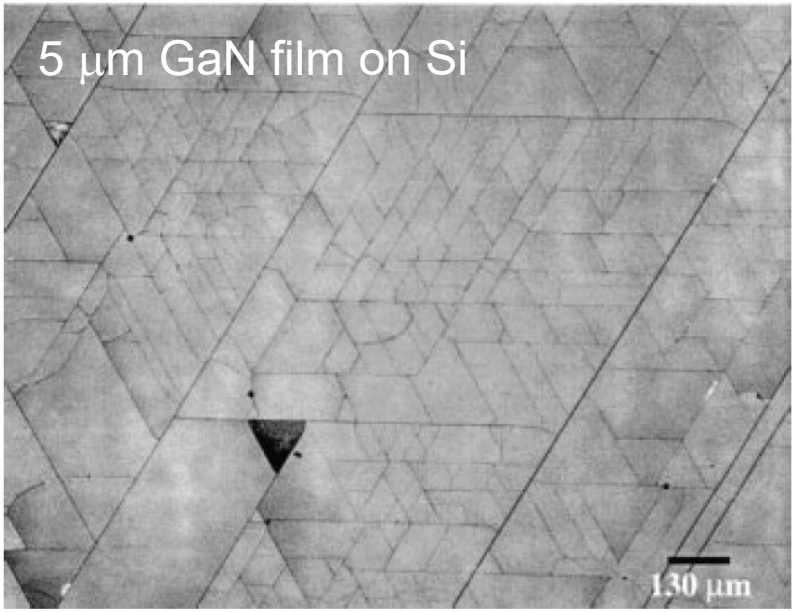


C. Coupeau , Thin Solid Films 406 (2002) 190–194

Introduction

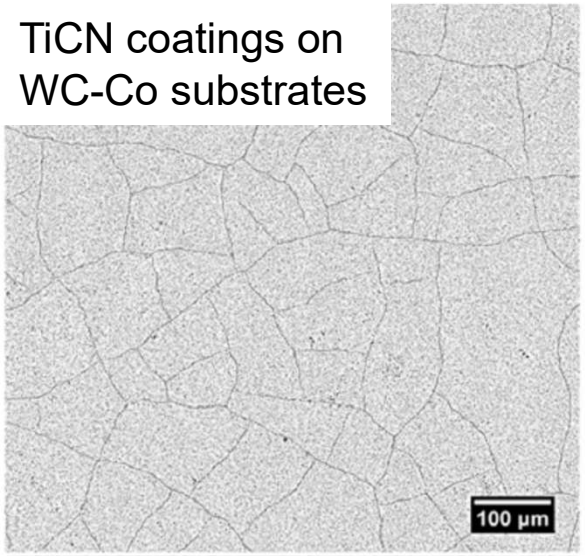
tensile stress





V.B. Shenoy, International Journal of Fracture ***109:*** *29–45 (2001)*

TiCN coatings on WC-Co substrates

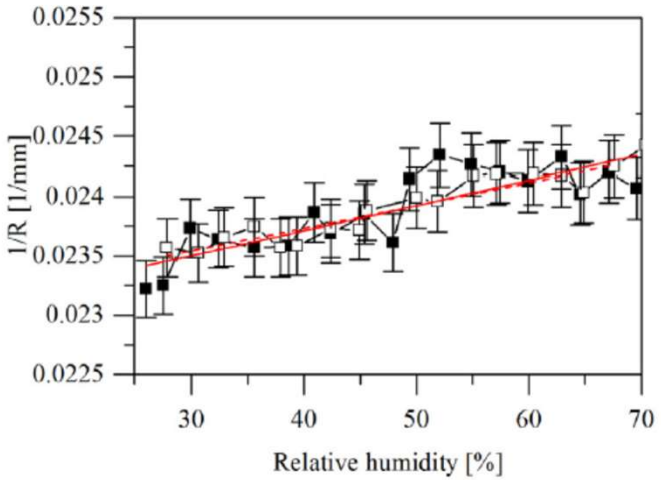


Stylianou et al, Int. J. Met. Refrac. Comp. ***86*** *(2020) 105102*

Introduction

Influence of external conditions

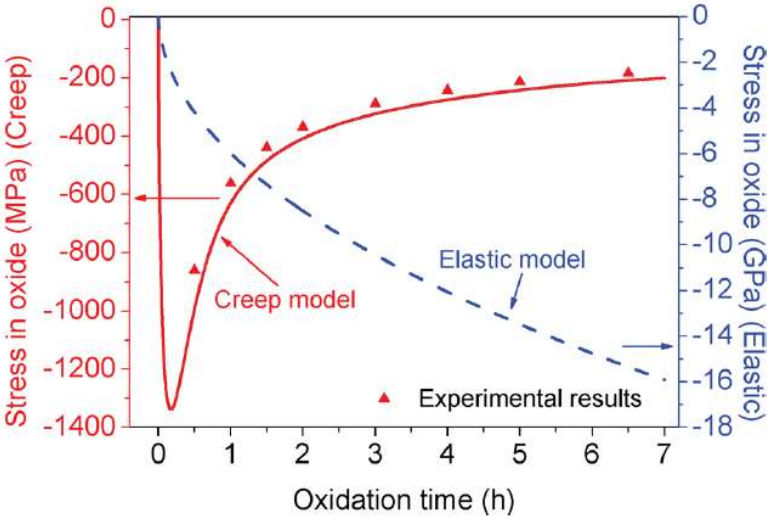
- **Exposure to humidity**



Top et al., SCT 347 (2018) 46

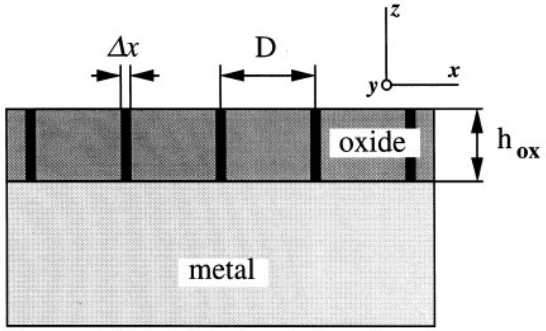
- Reversible increase of coating stress with humidity
- Possibility to derive the hygroscopic expansion

- **Isothermal oxidation**



Dong et al., JAP 112, 023502 (2012)

lateral growth strain of the oxide
+ creep strain of the oxide and metal



Tolpygo et al., Acta mater. 46 (1998) 927

Outline

- ✓ Introduction
- ✓ Origins of residual stress in PVD thin films
- ✓ Stress measurements methods: a brief description
- ✓ Stress evolutions during polycrystalline film growth
- ✓ Stress models
- ✓ Conclusions

Physical origins of stresses in thin films

Stress sources

- Usually, three stress components are distinguished

$$\sigma_{tot} = \sigma_i + \sigma_{th} + \sigma_{ext}$$

- Thermal stress σ_{th}

difference in thermal expansion coefficient between film and substrate and when $T_s \neq T_{amb}$

- Intrinsic stress σ_i

Stress source introduced during the PVD process: growth stress, coherency stress

- Extrinsic stress σ_{ext}

Induced by external factors: external loading, lifetime service, exposure to environment

Stress sources

- Usually, three stress components are distinguished

$$\sigma_{tot} = \sigma_i + \sigma_{th} + \sigma_{ext}$$

- Thermal stress σ_{th}

difference in thermal expansion coefficient between film and substrate and when $T_s \neq T_{amb}$

- Intrinsic stress σ_i

Stress source introduced during the PVD process: growth stress, coherency stress

- Extrinsic stress σ_{ext}

Induced by external factors: external loading, lifetime service, exposure to environment

Originates from strained regions
- ***within the film*** due to any micro-structural modification (grain boundaries, dislocation, voids), defects formation (point-defect, impurities, etc)
- *at the* ***film/substrate interface*** (lattice mismatch, intermixing, growth mode)
- *at the* ***film/vacuum interface*** (surface stress, adsorption)
- as a result of **dynamic** processes (interdiffusion, recrystallisation, etc…)

Table 8–1 Some possible sources of intrinsic stress classified according to the location where it exerts in the film.

Intrinsic stress sources	Location of stress source: Film/substrate interface	Film bulk	Free surface	Remarks	References
Tensile					
Crystallite coalescence	✓		✓	Cohesive forces upon GB formation	[48–50]
Attraction between columns		✓		Cohesive forces, shrinkage of GB voids	[51–54]
Void formation		✓			[53,55]
Grain growth		✓		GB area reduction, film densification	[56–58]
Structural phase change		✓		For example, amorphous to crystalline (Mo) or A15 to bcc (W and Ta)	[34–37]
Coherence stress	✓			Depends on lattice mismatch	[59]
Film roughening and shadowing			✓	For example, during film thickening or at glancing angle deposition	[52,60]
Compressive					
Capillary–induced stress			✓	Submonolayer coverage, isolated islands, continuous film	[61–63]
Excess population of adatoms			✓	For example, at surface ledges or terraces	[64–66]
Trapping of adatoms at GB		✓		Driven by chemical potential gradients and entropic effects	[67,68]
Atomic peening: incorporation of excess atoms and structural damage		✓		In the grain interior or at GB	[51,69,70]
Impurity incorporation			✓	Adsorption–induced change in surface stress	[71–73]
		✓		At lattice sites or at GB	[74]
Metastable phase formation	✓			For example, bcc Ti in W/Ti multilayers	[75]
Coherence stress	✓			Depends on lattice mismatch	[59]

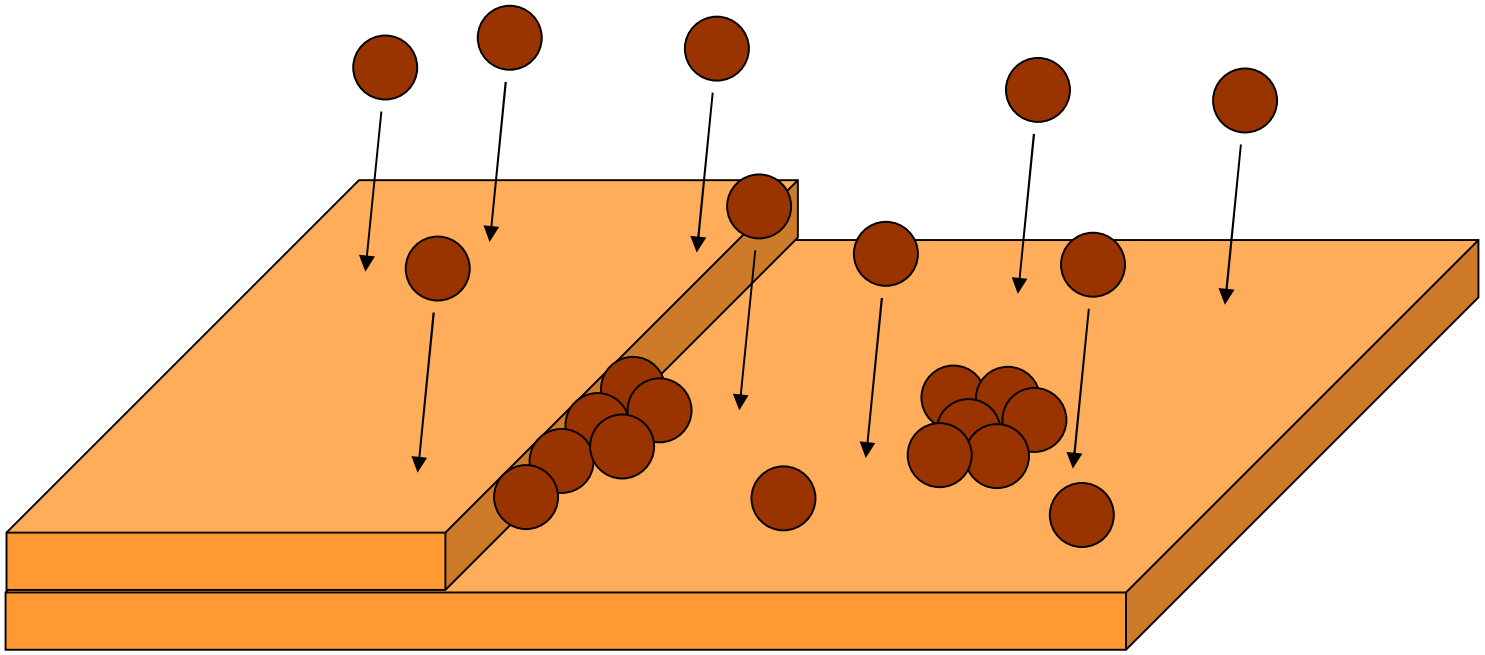
GB, Grain boundary.

from Abadias and Daniel, Chapter 8 "Stress in physical vapor-deposited thin films: measurement methods and selected examples", Handbook of Modern Coating Technologies, Elsevier, 2021

Stress and dynamics of film growth

during growth - surface different than eq. (much larger incoming flux than outgoing)

Ag: 23 C, 0.1 nm/sec → P(vapor)/P(equilibrium) = 10^{38}

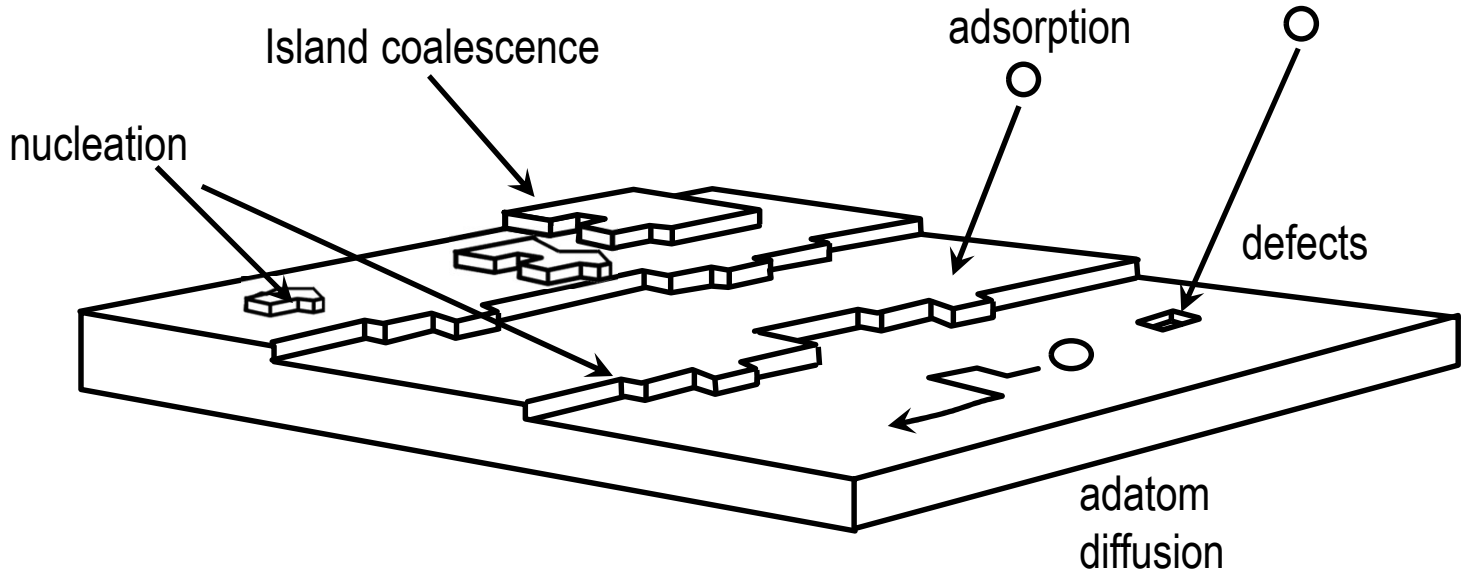


Supersaturation of adatoms during growth → *Higher chemical potential than equilibrium* → *High density of adatoms/clusters*

Stress and dynamics of film growth

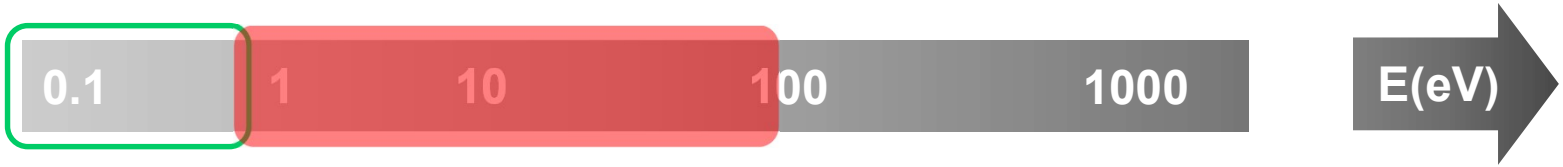


thermal evaporation

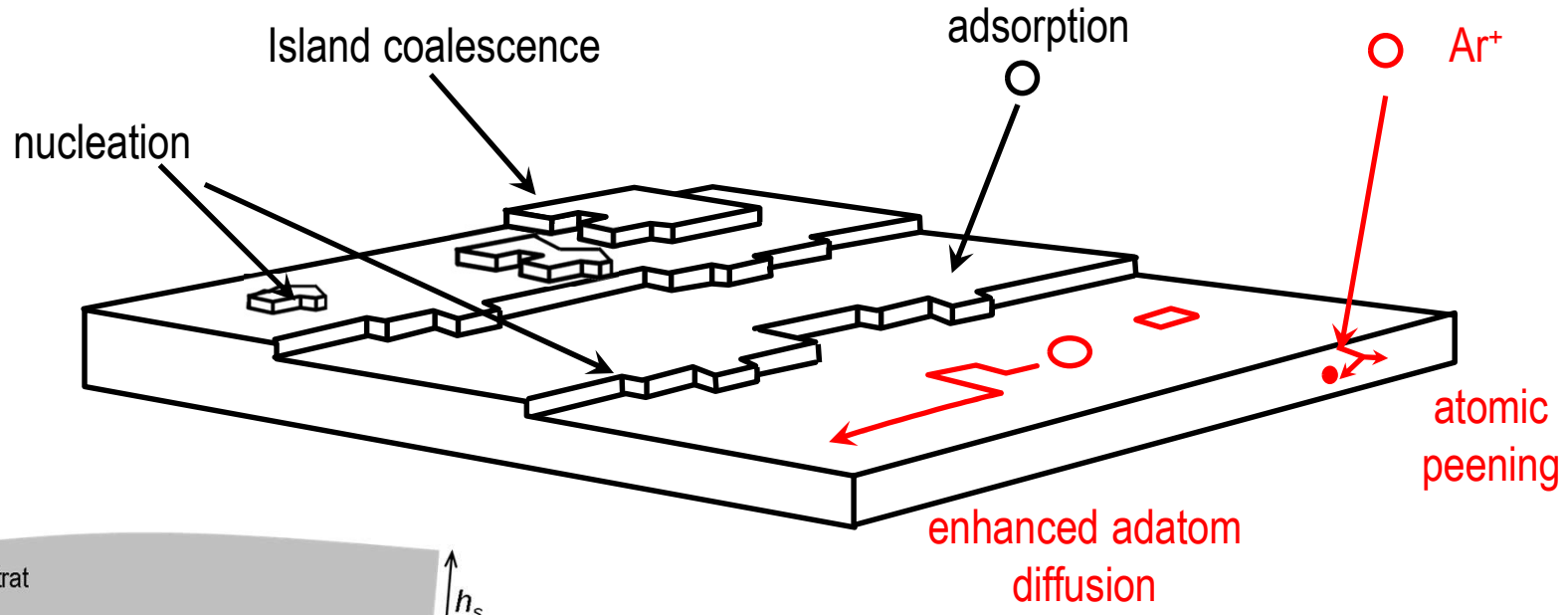


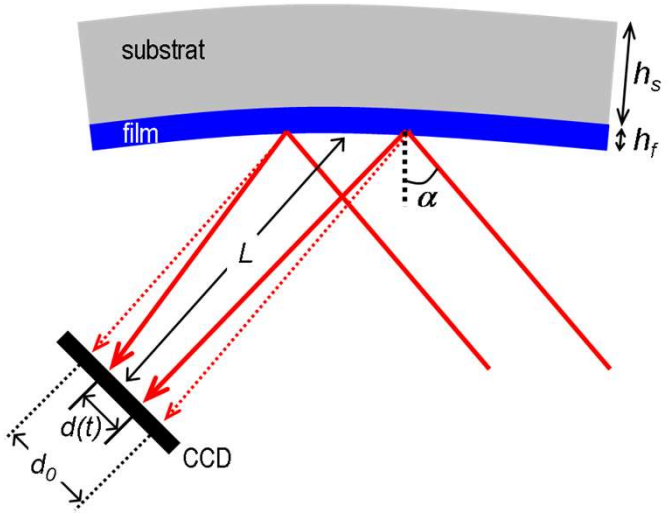
Elementary growth processes

Stress and dynamics of film growth



thermal evaporation *magnetron sputtering*





Fundamental understanding of growth mechanisms

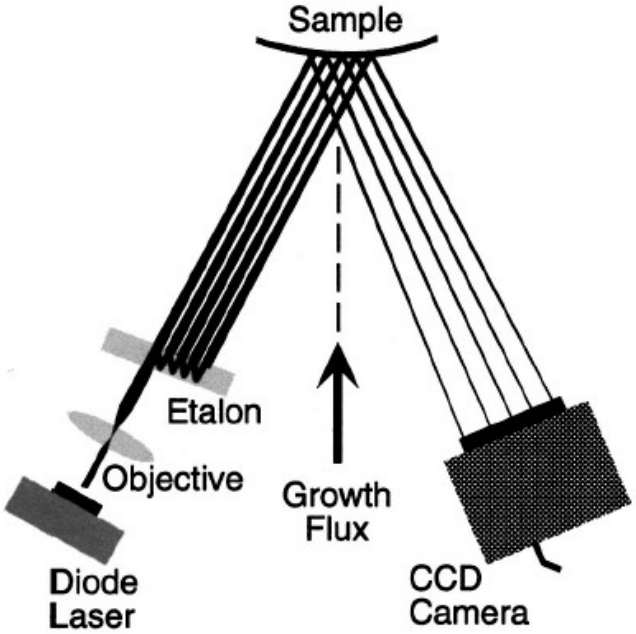
- **early growth stages** (nucleation/coalescence)
- **growth dynamics using real-time techniques** (wafer curvature, surface differential reflectivity, RHEED, …

Experimental determination of stress in thin films

How measuring residual stress (or strain) in thin films ?

'wafer curvature' method

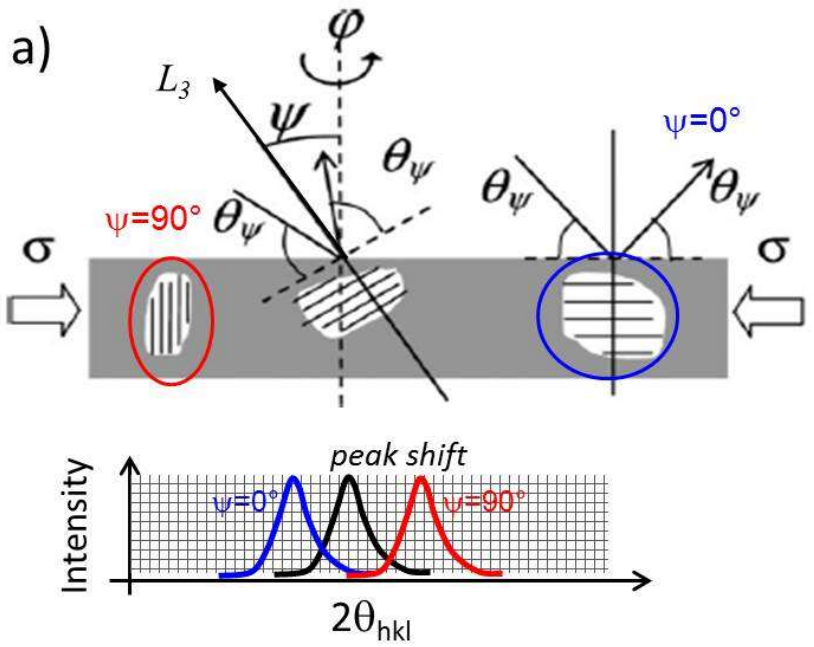
⇒ integrated (macroscopic) stress
⇒ in-situ diagnostic



Floro et al., JAP 89 (2001) 4886

X-ray Diffraction

⇒ internal (microscopic) strain gauge
⇒ in-situ diagnostic
⇒ limited to crystalline materials

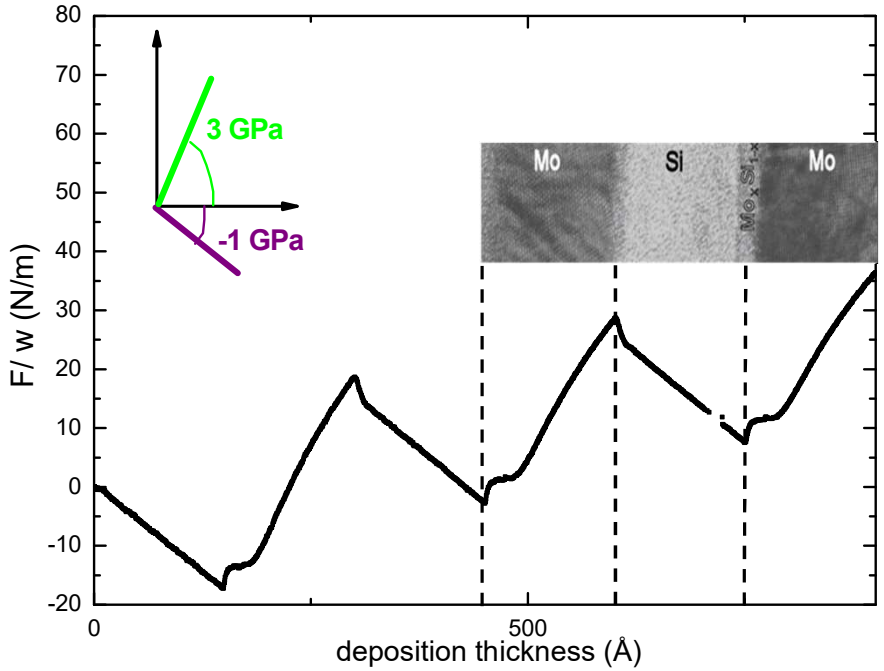


Welzel et al., J. Appl. Crystal. 38, 1 (2005)

Potentialities offered by curvature technique

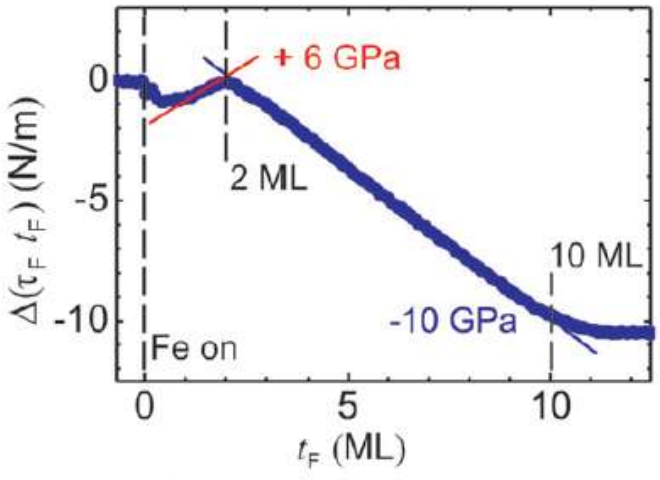
- No need to know the elastic properties of the studied material
- Stress can be measured in **amorphous** (sub)layers
- ***In situ* stress** monitoring during growth can be easily implemented
- **High sensitivity** (sub-nm scale): surface and interface stress can be uncovered
- Phase transition can be observed in real-time

Mo/Si multilayers



A. Fillon, PhD Thesis, Univ. Poitiers (2010)

Fe on Ir (001)

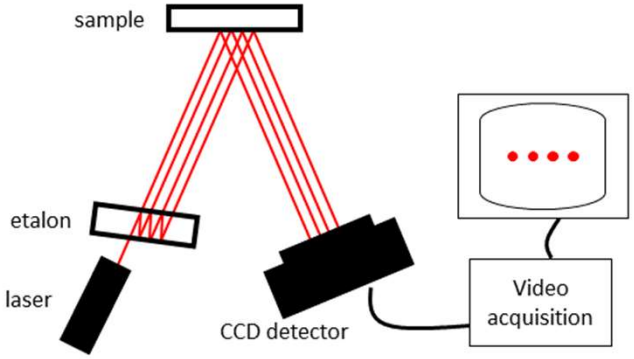


D. Sander et al., J. Phys.: Condens. Matter 21 (2009) 134015

Available commercial tools for in situ stress monitoring

Laser deflection : Use the deflection of one (or a matrix of parallel) laser beam(s) by the wafer surface





E. Chason et al. Surf. Engin. 19-5 (2003 ,387

Relative spot spacing

Curvature: $\Delta\kappa(t) = -\frac{\delta d(t)}{d_0}\frac{\cos\alpha}{2L}$

kSA MOS

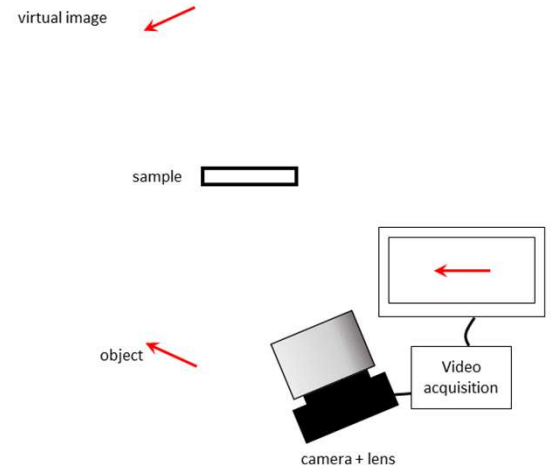
LAYTEC Knowledge is key

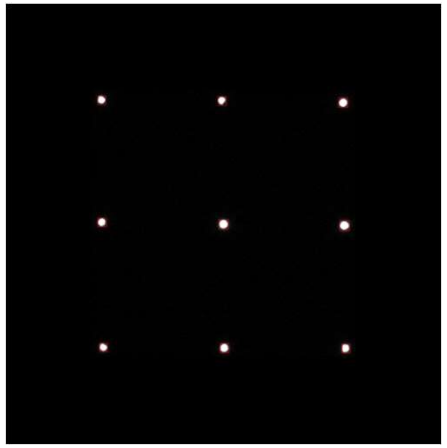
EpiCurve® TT

Available commercial tools for in situ stress monitoring

Virtual image magnification analysis : MIC (Magnification Inferred Curvature) measures the magnification factor of a virtual image created by a surface







Curvature = f(magnification factor)

Highly stable and alignment-free measurements
High rate capability (100FPS)

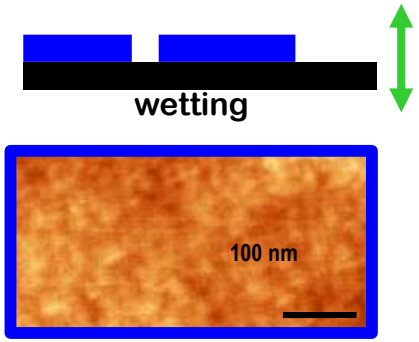
RIBER
EZ-CURVE

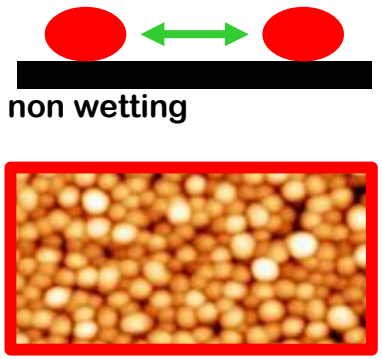
A. Arnoult and J. Colin, Sci. Rep. 11 (2021) 9393
LAAS-CNRS - Université de Toulouse, France

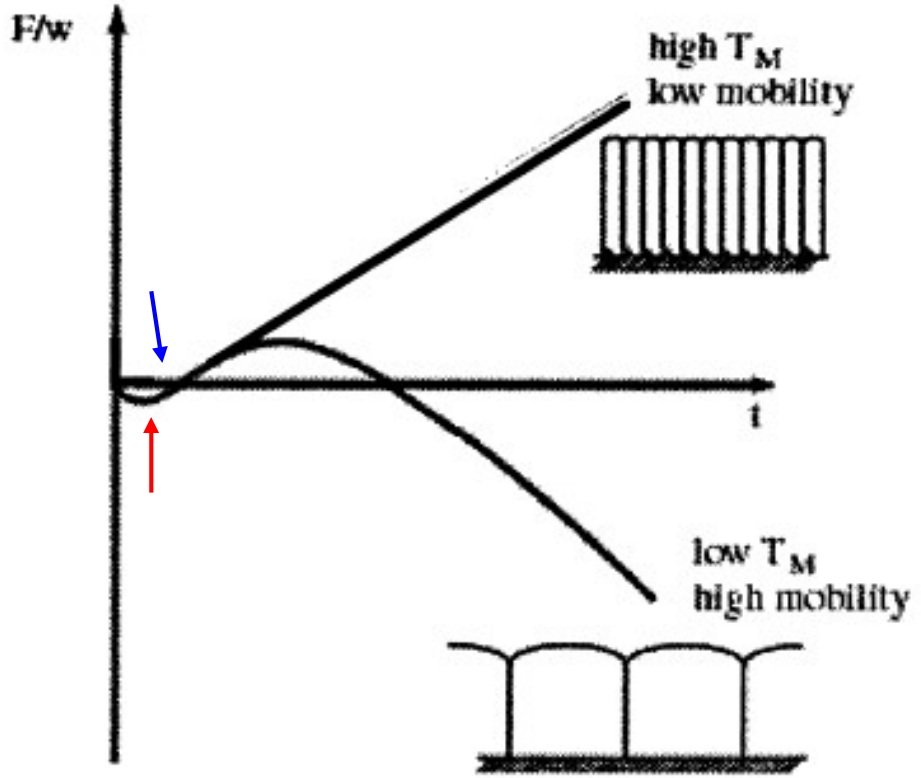
Intrinsic stress evolution during polycrystalline thin film growth

Archetypal stress evolution

Two archetypes of stress evolution







Co	1768 K
Fe	1811 K
Ti	1941 K
Mo	2896 K

Al	933 K
Ag	1235 K
Au	1337 K
Cu	1357 K

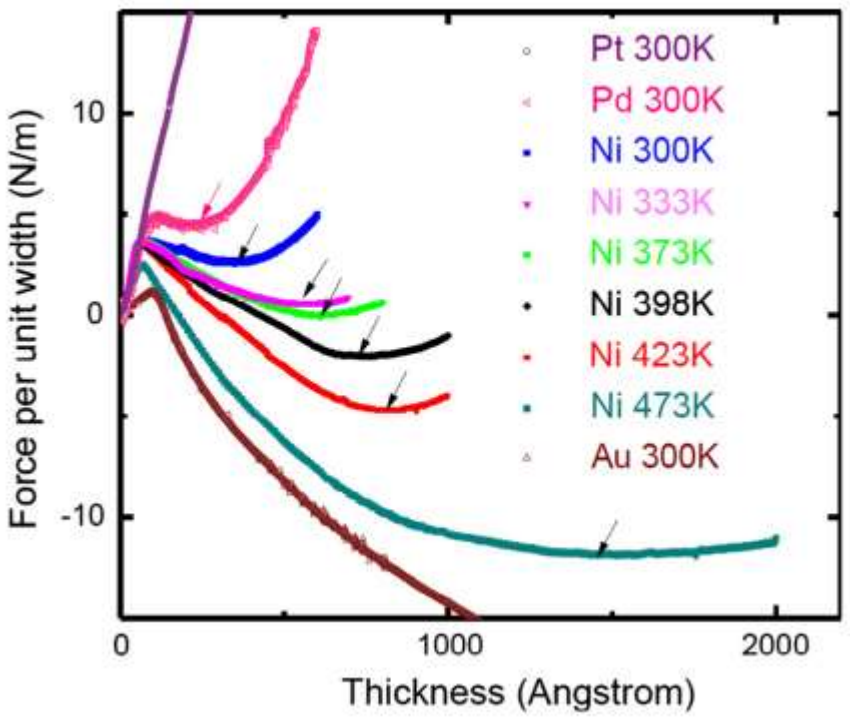
Schematic drawing for metal films grown by thermal evaporation

Archetypal stress evolution

Depending on the material mobility (or homologous temperature T_s/T_m), the force evolution may be more complex

- For **intermediate** adatom mobility, like Ni or Pd evaporated films, a **stress turnaround** is observed in the later stages, where the instantaneous stress changes from compressive to tensile

- The turnaround thickness increases as the substrate temperature is increased or the deposition rate is decreased

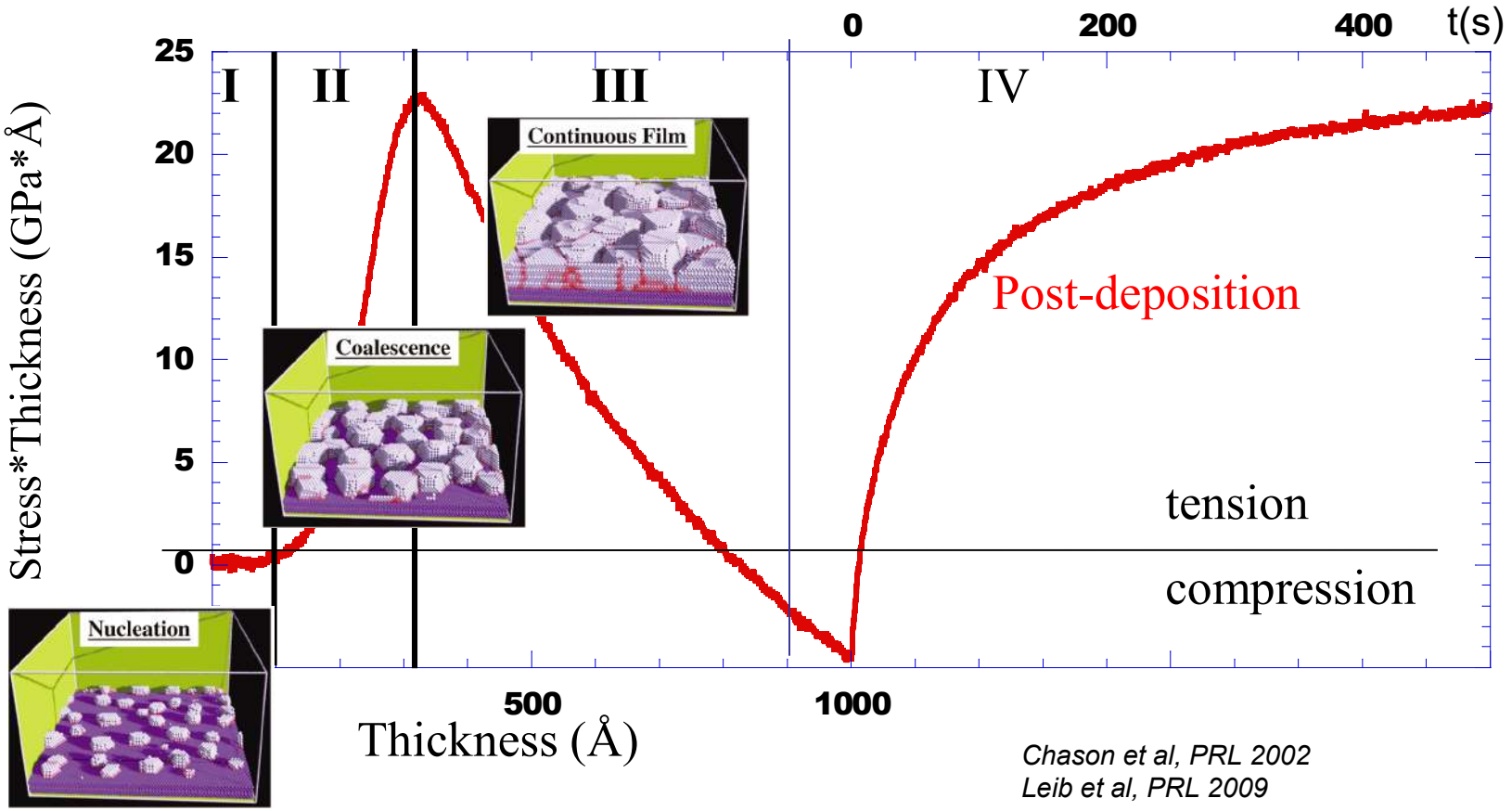


from H.Z. Yu, C.V. Thompson, Acta Materialia 67 (2014) 189

Volmer-Weber (3D) growth mode of high-mobility metal: Ag on Si

compressive-tensile-compressive (CTC) behavior

⇒ typical of high-mobility metals growing in Volmer-Weber mode



Chason et al, PRL 2002
Leib et al, PRL 2009

Floro et al. JAP (2001)
Abermann and Koch (1986)
Shull and Spaepen (1996)
Gonzalez-Gonzalez, PRL (2013)

- Reversible stress change upon growth interrupt

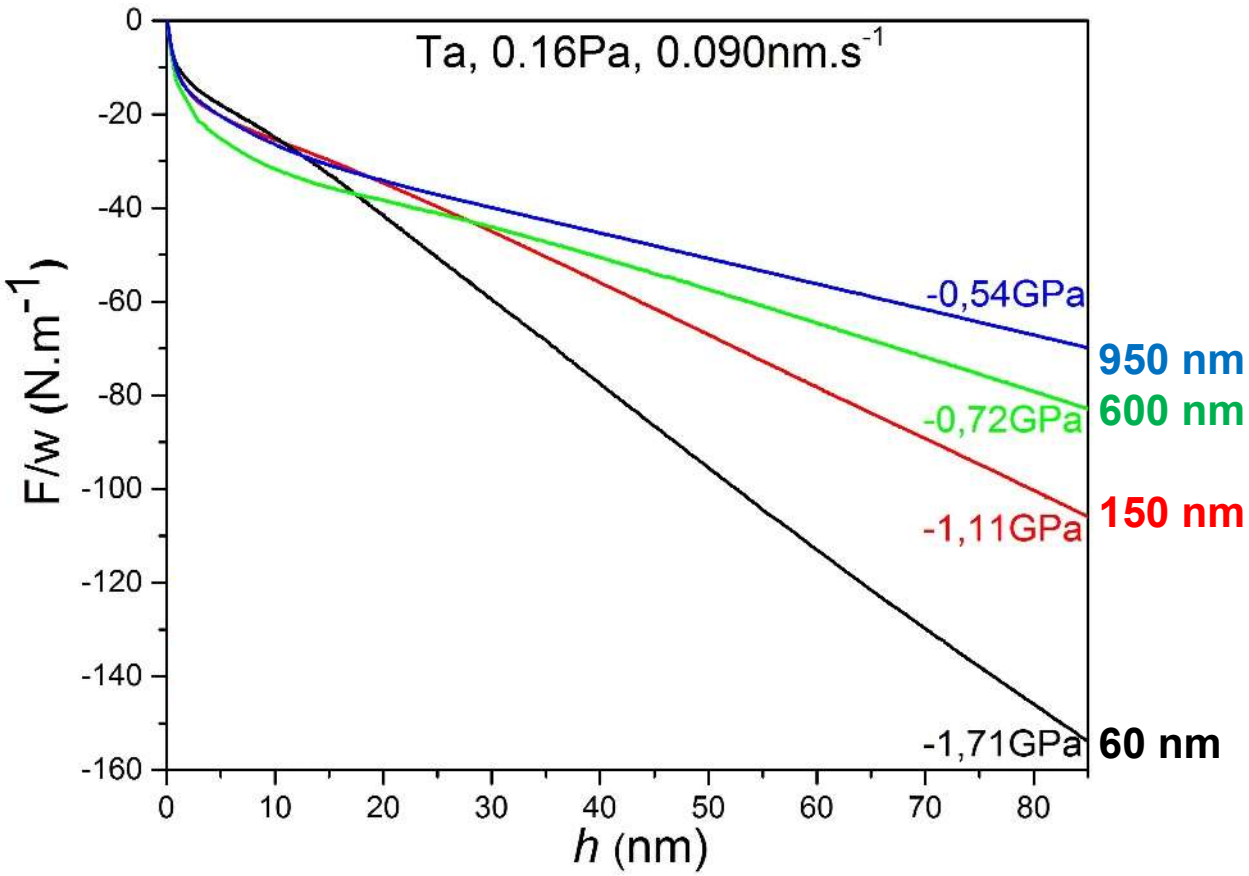
⇨ Spontaneous flow of excess atom at the GB ?

⇨ Morphological rearrangement ?

Stage III: continuous film growth - role of grain boundary

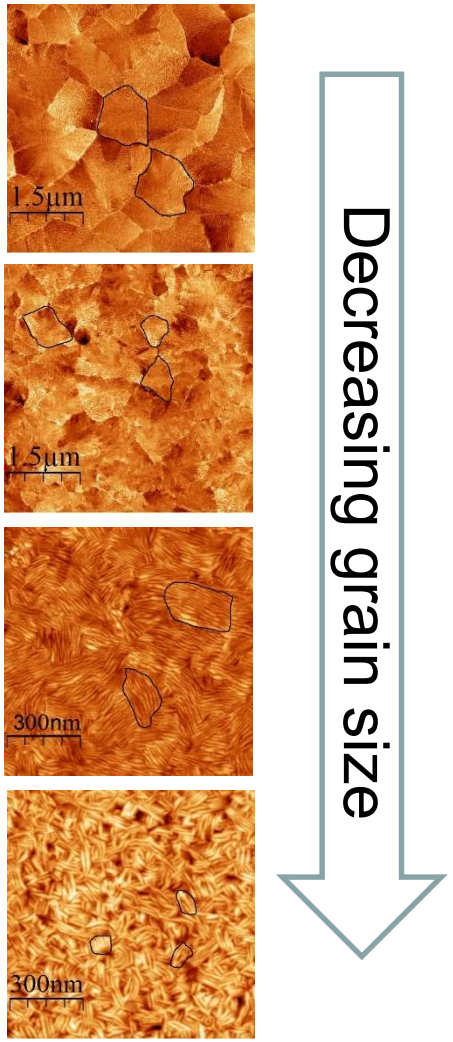
Ta films sputter-deposited on crystalline template layers with controlled grain size

▪ ***In situ* stress measurement**



Higher compressive stress with smaller grain size

▪ **AFM images h_{Ta} = 100nm**

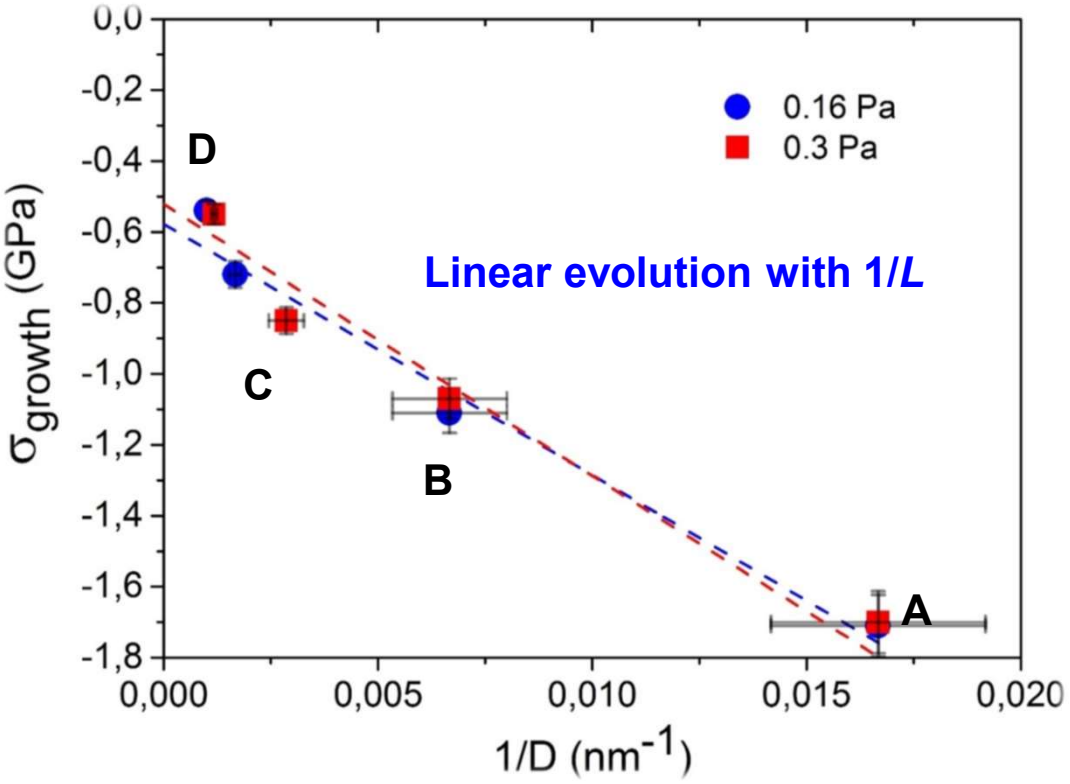


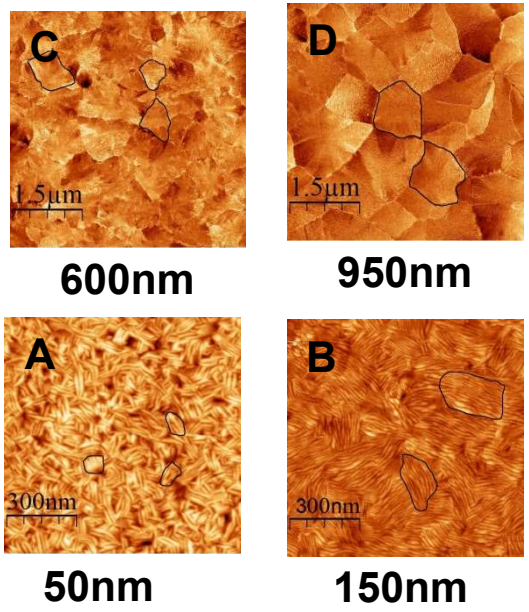
In collaboration with K. Sarakinos, IFM Linköping (Sweden)

Stage III: continuous film growth - role of grain boundary

Ta films sputter-deposited on crystalline template layers with controlled grain size

GB density: $\frac{\pi * D}{\pi * D^2/4} \propto \frac{1}{D}$





from J. Colin, PhD Thesis, Univ. Poitiers, France (2015)

Stress models

Models of stress formation and evolution – continuous regime

Different models have been proposed to describe and predict stress evolution during the post-coalescence regime

- **Kinetic model of Chason**

  Diffusion of excess atoms at the GB due to non-equilibrium growth conditions

$$\sigma_{tot}(L,R,T) = \sigma_T + \sigma_c + \sigma_{gg} + \sigma_{Edep}$$

Coalescence (*tensile*) | Incorporation at GB (*compressive*) | Grain growth (*tensile*) | Energertic bombardement (*tensile*)

L= grain size
R= deposition rate
T= temperature

- **Capillary model of Vasco & Polop**

  Out-of-equilibrium surface profile during deposition
  Surface stress (Laplace pressure) due to difference in *surface curvature* $\Delta\kappa(r)$

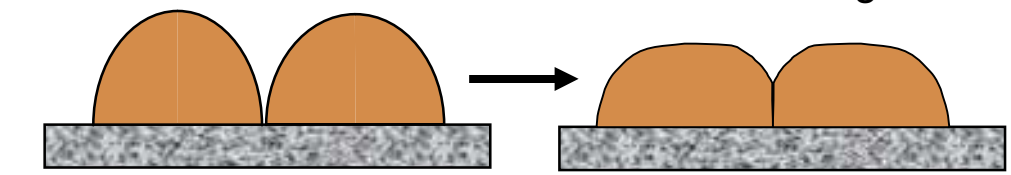
- **Model of Thompson – morphological change**

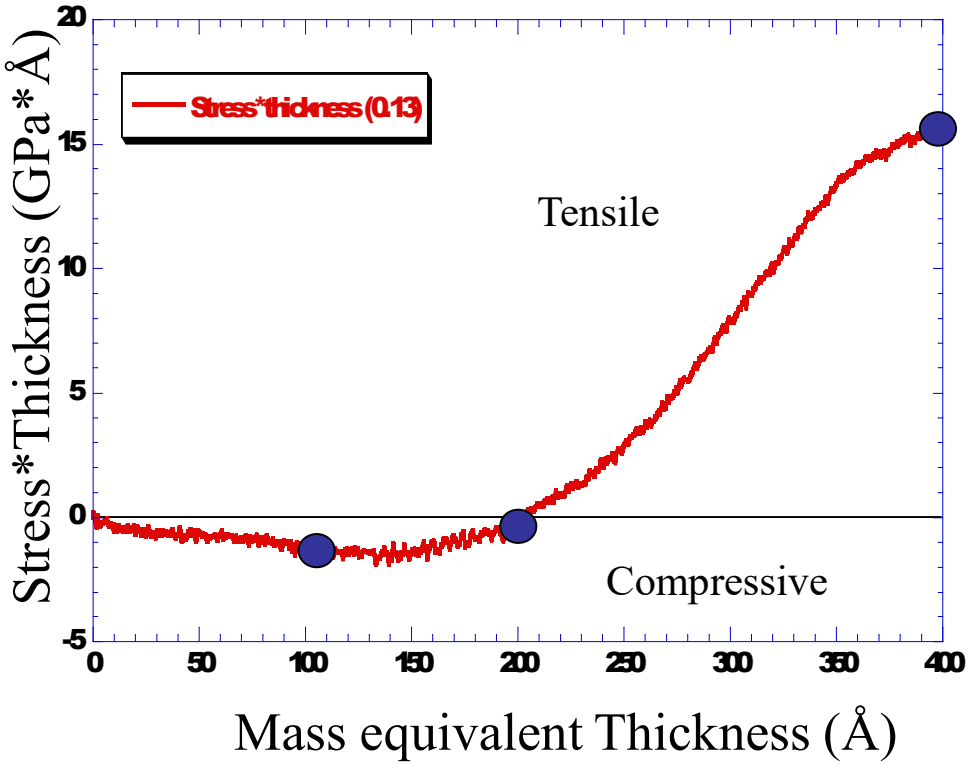
  Out-of-equilibrium surface profile during deposition
  Mass transport during growth interrupt to recover equilibrium profile

Stage II: attractive force during island coalescence

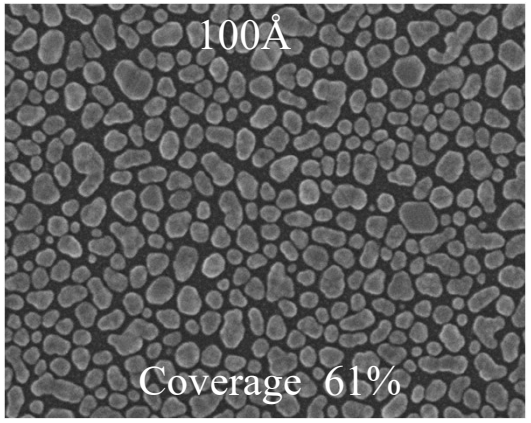
• Creation of grain boundaries during island coalescence induces tensile stress

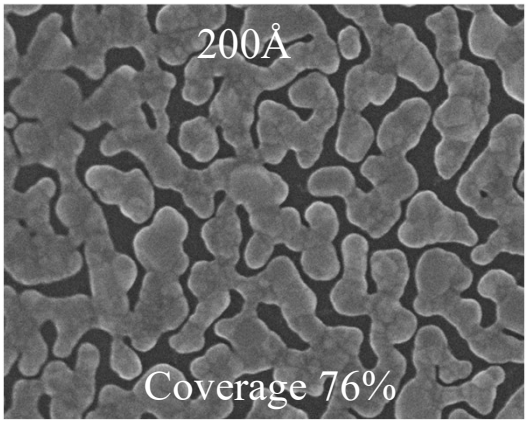
Ag films on SiO_2

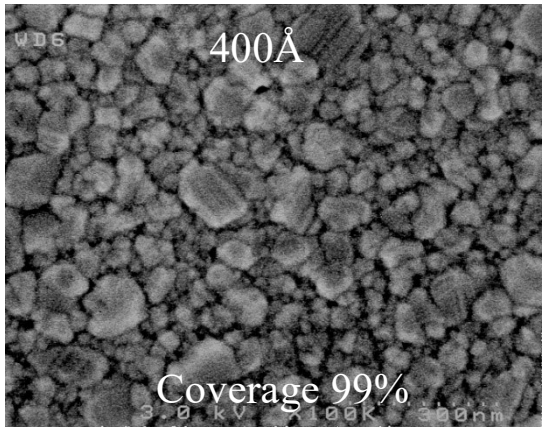




Courtesy of Eric Chason

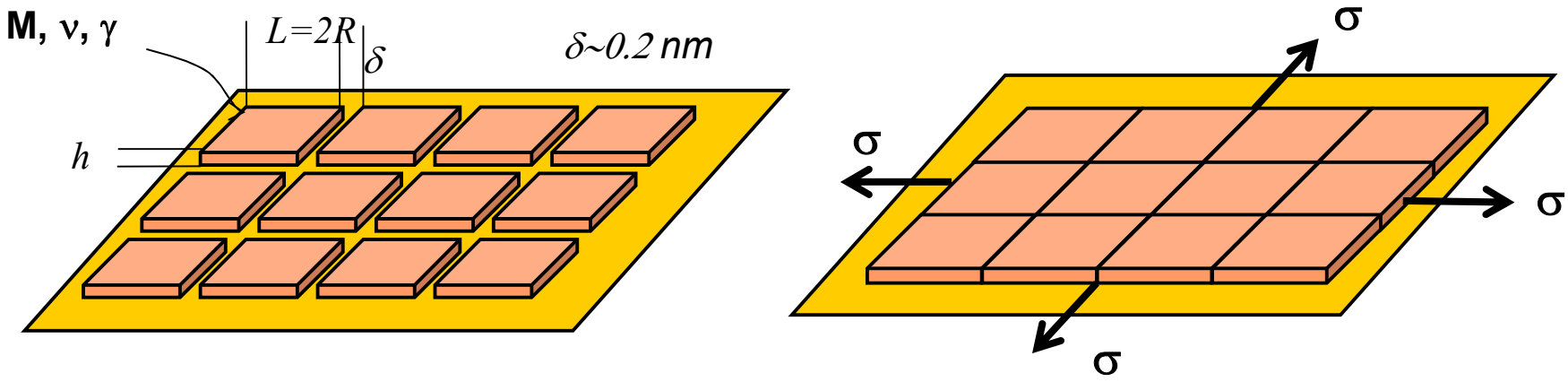






Stage II: origin of tensile stress upon island coalescence

- Free surfaces convert to grain boundaries at expense of strain energy
- Driving force: surface energy gain: $\gamma_{gb} - 2\gamma_s < 0$



from R.W. Hoffman, Thin Solid Films 34 (1976) 185

Energy balance between

- Increase in strain energy $\Delta E_{\text{strain}} = hL^2 \frac{\sigma^2}{\left(\frac{E}{1-\nu}\right)}$.
- Decrease in surface energy $\Delta E_{\text{interface}} = -4Lh\Delta\gamma$

$$\Delta\gamma = \gamma_s - \frac{1}{2}\gamma_{gb} > 0$$

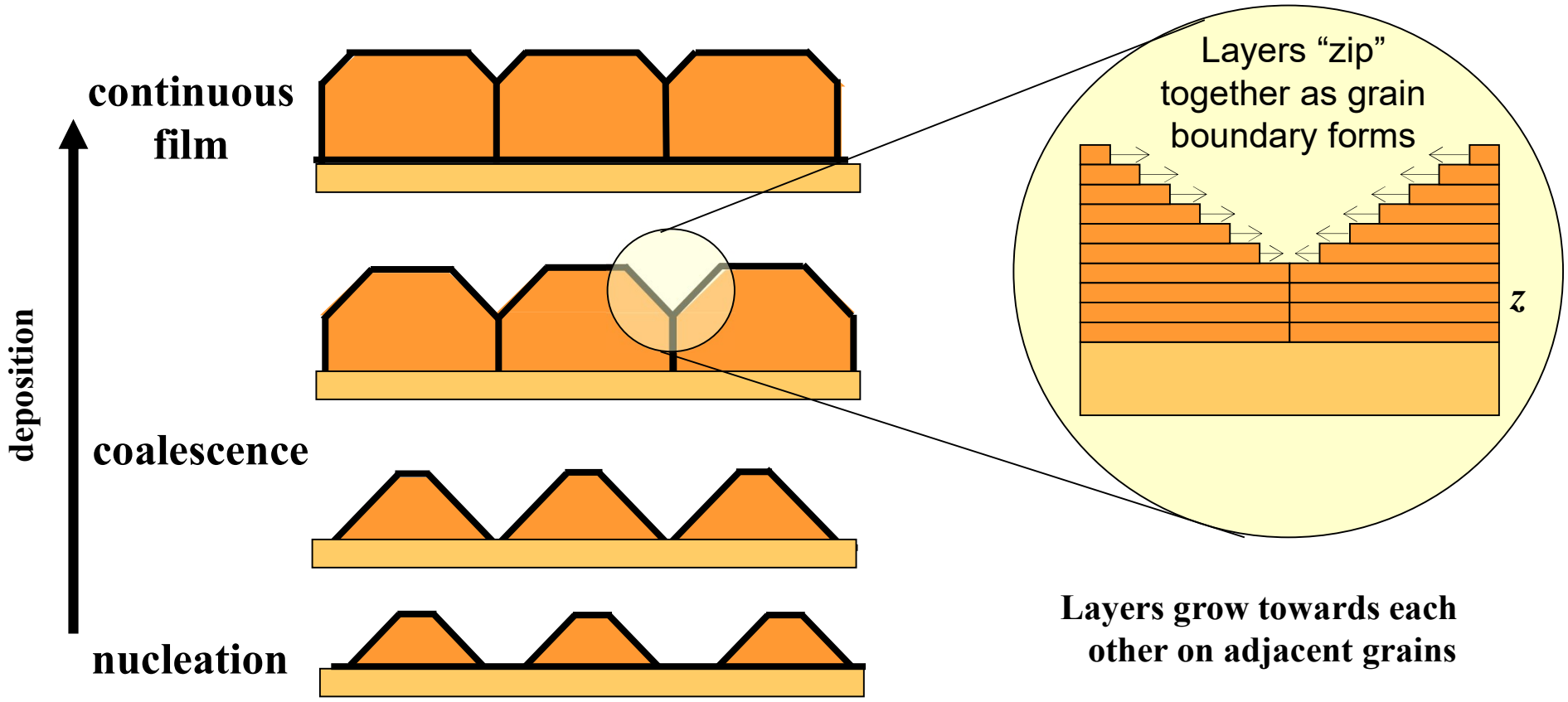
This model predicts a critical value for tensile stress

$$\sigma_{crit} = 2\sqrt{\frac{Y_f \Delta\gamma}{L}}$$

→ 1-2 GPa!

The dependence on $L^{-1/2}$ suggests that **finer-grained materials** will have **larger tensile stress** generated due to more grain boundaries formed per unit area of film
But this model largely overestimates experimental tensile stress values, and it considers an unrealistic geometry of grain boundary formation

Stage II: origin of tensile stress upon island coalescence



Attractive force between atoms makes grain boundary "snap" closed, and creates residual tensile stress

Stage III: kinetic model of defect incorporation into GB

Kinetic (diffusion-based) model proposed by E. Chason (2002-2020)

➲ Origin: non-equilibrium conditions on the film surface

- Increase chemical potential at the surface due to oversaturated vapor flux

$$\mu_s = \mu_s^0 + \delta\mu_s.$$

driving force for diffusion

- Chemical potential of the grain boundary

$$\mu_{gb} = \mu_{gb}^0 - \sigma\Omega$$

- Chemical potential difference

$$\Delta\mu = \mu_s - \mu_{gb} = \Delta\mu_0 + \delta\mu_s + \sigma\Omega$$

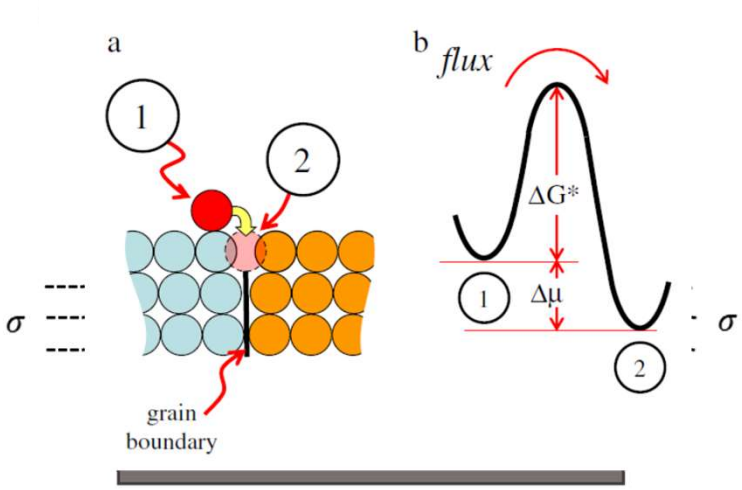
- Adatom diffusion into the triple junction will change the strain in the layer

$$\Delta\epsilon_i = -\frac{N_i a}{L}$$

(valid for low-mobility materials)

- Stress generated in layer i

$$\sigma_i = \sigma_T + \sigma_C = \sigma_T - M_f \frac{N_i a}{L}$$



from *Chason et al., Phys. Rev. Lett. 88, (2002) 156103*
Chason, Thin Solid Films 526 (2012) 1
Chason & Guduru, JAP 119 (2016) 191101
Chason et al., JAP 119 (2016) 145307
Chason et al., JAP 123 (2018) 185305
Jagtap & Chason, Acta Mater. 193 (2020) 202

Stage III: kinetic model of defect incorporation into GB

- Rate of atoms diffusing into the triple junction

$$\frac{\partial N_i}{\partial t} = 2C_s \frac{2D}{a^2}\left(1 - e^{-\frac{\Delta\mu}{kT}}\right) \simeq 2C_s \frac{2D}{a^2}\frac{\Delta\mu}{kT} \quad \Rightarrow \quad \frac{\partial \sigma_i}{\partial t} = -\frac{4C_s M_f}{akT}\frac{D}{L}(\sigma_i \Omega + \delta\mu_s)$$

- C_s is the dimensionless concentration (fractional coverage) of mobile atoms on the surface that are free to make diffusive jumps into the triple junction
- *D* is an effective diffusivity related to the rate of hopping, i.e., the rate of transition between the free surface and the grain boundary

The solution of this equation has the form

$$\sigma_i = \sigma_C + (\sigma_T - \sigma_C)e^{-\beta\frac{D}{RL}}.$$

σ_T = tensile stress due to coalescence $\quad \sigma_T \propto L^{-1/2}$

σ_C = compressive stress due to insertion of atoms at the GB

for the ***steady-state regime*** for which the grain boundary velocity equals a/*R*

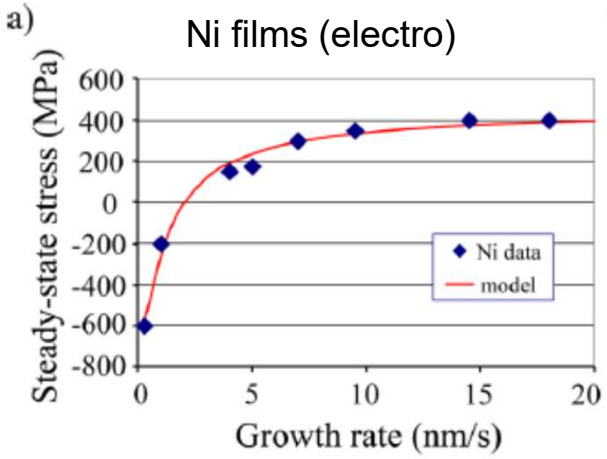
- when *D/RL* is **large** (i.e., high effective diffusivity or low growth rate), the stress is predicted to be compressive with a maximum value of σ_C .
- when *D/RL* is **small** (i.e.,low effective diffusivity or high growth rate), there is not sufficient time for atoms to be inserted into the triple junction and a net tensile stress is generated as the grain boundary forms.

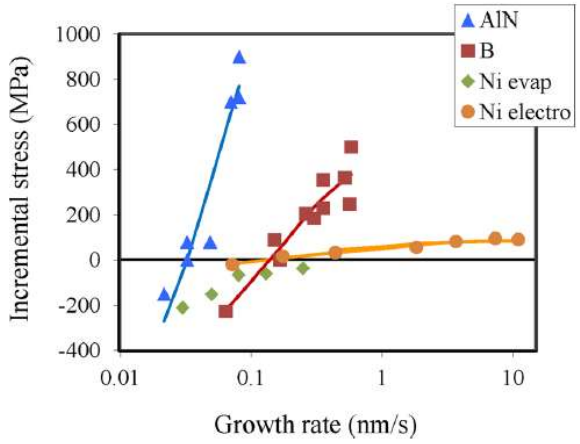
- The model predicts higher compressive stress for smaller grain size

Stage III: kinetic model of defect incorporation into GB

Results of the model

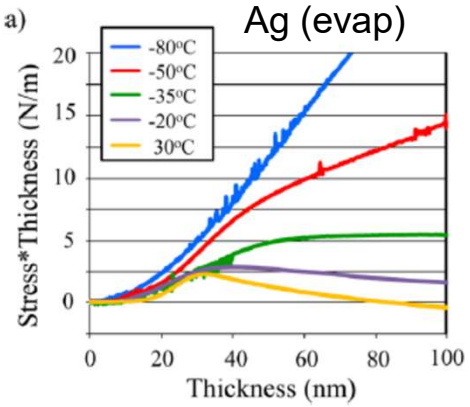
Influence of growth rate

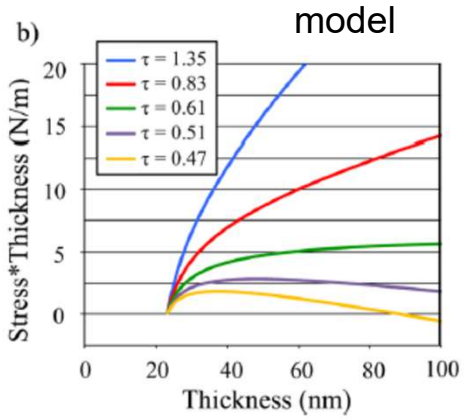




Chason & Guduru, JAP 119 (2016) 191101

Influence of temperature





$$\sigma_C \equiv \frac{-\delta\mu_S}{\Omega},$$

$$\frac{1}{\tau} \equiv \beta\frac{D}{aL},$$

$$\beta \equiv \frac{4C_S M_f \Omega}{kT},$$

Chason et al., JAP 111 (2012) 083520

Stage III: Contribution of grain growth

- Effect of changing grain size L(z) on calculations of stress-thickness evolution during film growth.

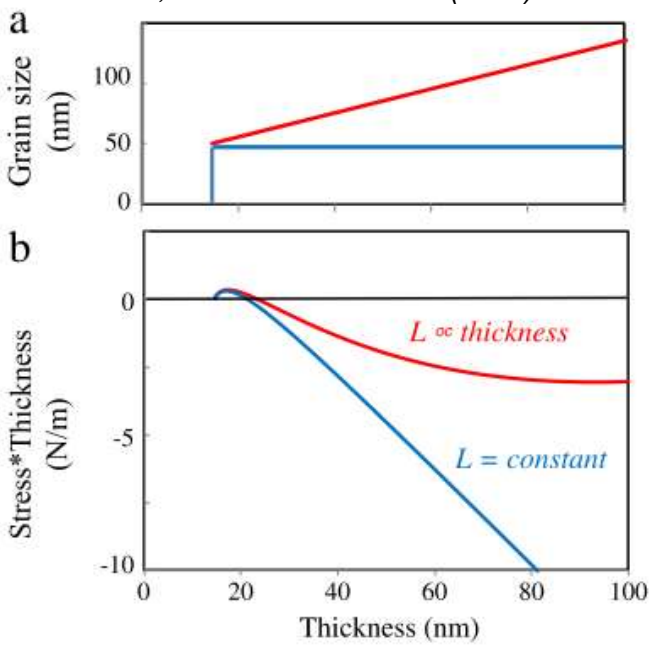
⇒ Eliminates GB

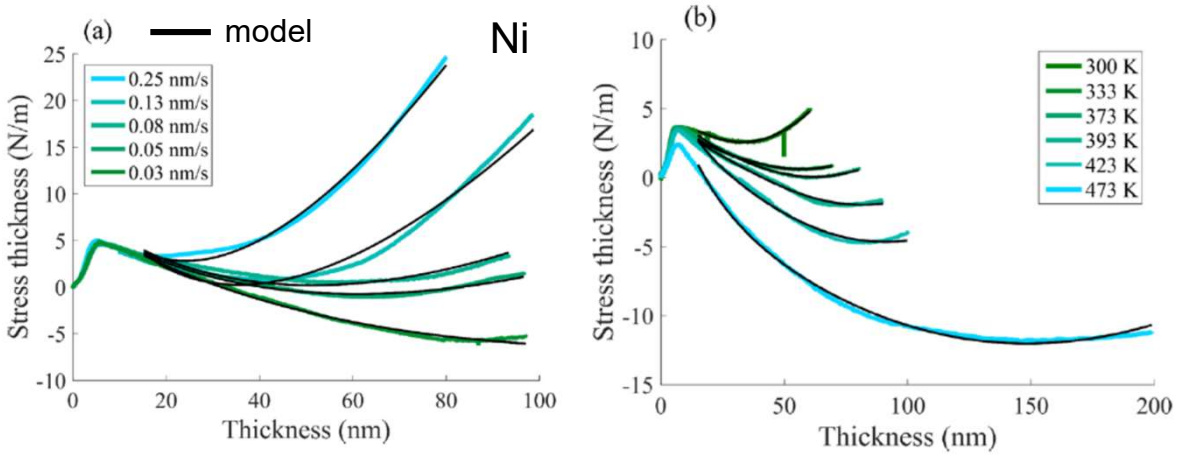
Grain growth corresponds to the developpment of a ***tensile stress*** component

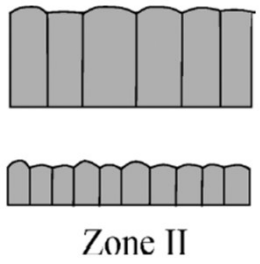
$$\left(\sigma \times h_f\right)_{gg} = M_f \, \Delta d \int_0^{h_f} \left(\frac{1}{L(z)} - \frac{1}{L(h_f)}\right) dz.$$

$\Delta d =$ excess volume per unit area (~0.1 nm)

E. Chason, Thin Solid Films 526 (2012) 1





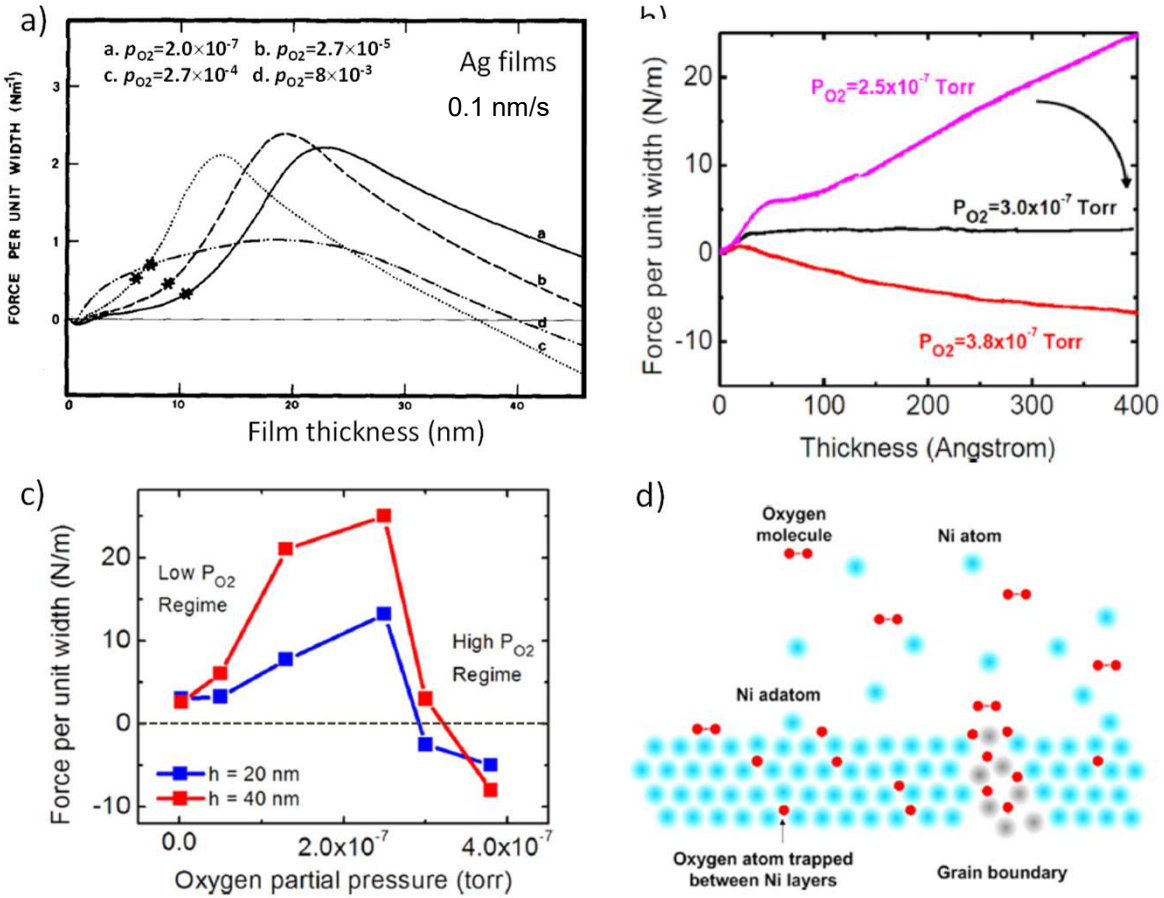


hypothesis: zone II regime and linear grain size increase $L = L_0 + \alpha \, h_f$

The model reproduces fairly well the experimental data on Ni films as a function of R and T

from Chason et al., JAP 123 (2018) 185305

Influence of oxygen partial pressure / impurity incorporation



- **Early stages**: Earlier onset of coalescence with increasin p_{O2}
- **Continous films**: Different stress regimes depending on p_{O2}
- **Competition** between tensile (grain growth) and compressive (lattice distortion and incorpo-ration of atoms at the GB) stress mechanisms
- **Chemisorbed O** atoms may also reduce diffusion length of Ni atoms

* Indicates percolation

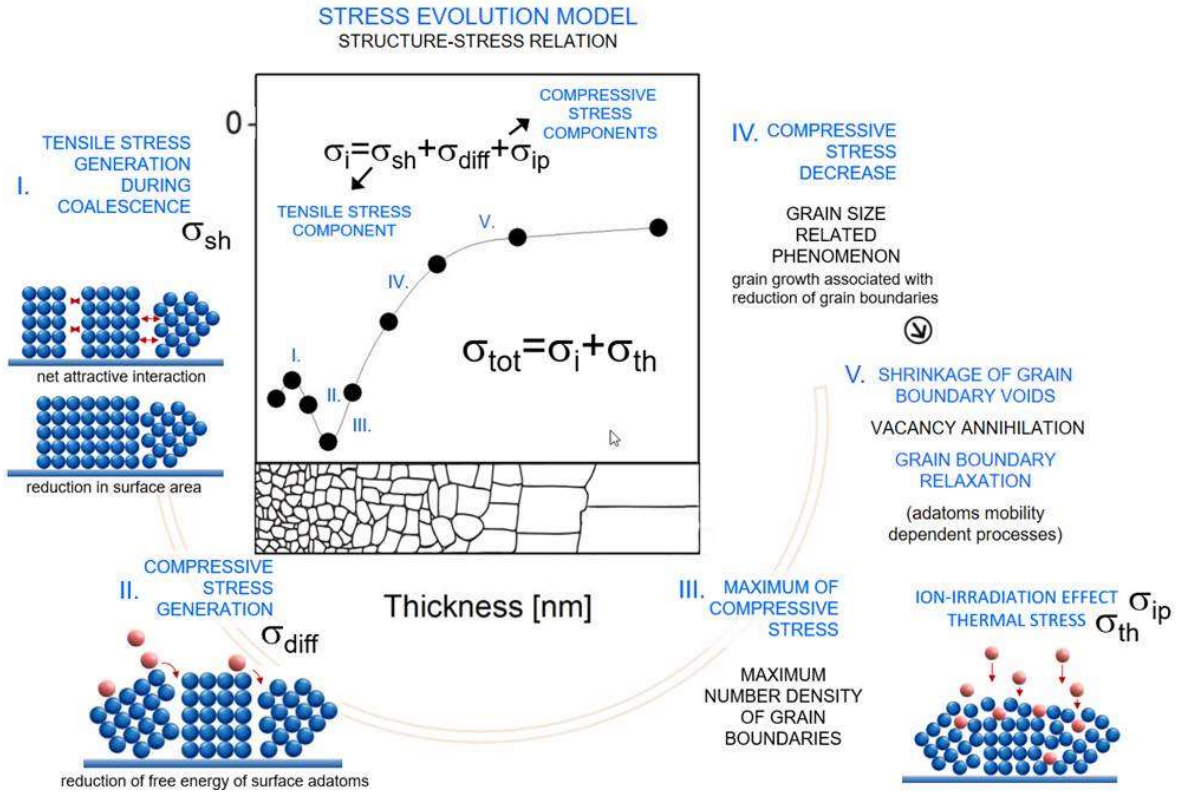
from a) Aberman & Koch, Thin Solid Films 142 (1986) 65
b)-d) Yu & Thompson, J. Vac. Sci. Technol. A 33 (2015) 021504

Impurity incorporation (oxygen or inert gas atoms) often contribute to compressive stress

Conclusions

- Coupling real-time diagnostics is a powerful methodology to better understand the early growth stages during thin film deposition

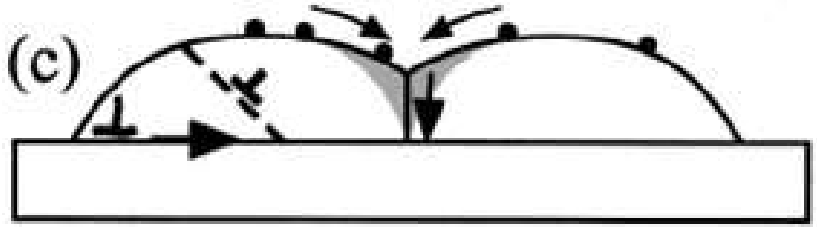
- Complex interplay between film formation processes, microstructure and stress: kinetics effects are dominant



Some possible stress relaxation mechanisms

Relaxation kinetics are strongly dependent on deposition temperature and microstructural length scales

- Interfacial shear for weak film/substrate interaction
- Inclined shear: dislocations on inclined glide planes
- Viscous flow in amorphous materials
- Surface diffusion : morphological rearrangement, Ostwald ripening, flow of adatoms in the GB



Floro et al., JAP 89 (2001) 4886

REVIEW ARTICLE

Journal of Vacuum Science & Technology A
36, 020801 (2018);

Review Article: Stress in thin films and coatings: Current status, challenges, and prospects

Grégory Abadias[a)]
Département de Physique et Mécanique des Matériaux, Institut Pprime, UPR 3346, CNRS-Université de Poitiers-ENSMA, SP2MI, Téléport 2, F86962 Futuroscope-Chasseneuil, France

Eric Chason[b)]
School of Engineering, Brown University, Providence, Rhode Island 02912-9104

Jozef Keckes[c)]
Department of Materials Physics, Montanuniversität Leoben and Erich Schmid Institute for Materials Science, Austrian Academy of Sciences, Leoben 8700, Austria

Marco Sebastiani[d)]
Engineering Department, University of Rome "ROMA TRE," Via della Vasca Navale 79, Rome 00147, Italy

Gregory B. Thompson[e)]
Department of Metallurgical and Materials Engineering, The University of Alabama, P.O. Box 870202, Tuscaloosa, Alabama 35487-0202

Etienne Barthel[f)]
Laboratoire Sciences et Ingénierie de la Matière Molle, ESPCI Paris, PSL University, Sorbonne Université, CNRS, F-75005 Paris, France

Gary L. Doll[g)]
Mechanical Engineering Department, The University of Akron, Akron, Ohio 44325-0406

Conal E. Murray[h)]
IBM T.J. Watson Research Center, Yorktown Heights, New York 10598

Chris H. Stoessel[i)]
Eastman Chemical Co., 3788 Fabian Way, Palo Alto, California 94303

Ludvik Martinu[j)]
Department of Engineering Physics, Polytechnique Montréal, Montreal, Quebec H3T 1J4, Canada

(Received 3 November 2017; accepted 9 February 2018; published 5 March 2018)